Inorg. Chem. **2009**, *48*, 4306−4316

Cyclometalated 6-Phenyl-2,2′-bipyridyl (CNN) Platinum(II) Acetylide Complexes: Structure, Electrochemistry, Photophysics, and Oxidative- and Reductive-Quenching Studies

Jacob Schneider, Pingwu Du, Paul Jarosz, Theodore Lazarides, Xiaoyong Wang, William W. Brennessel, and Richard Eisenberg*

Department of Chemistry, University of Rochester, Rochester, New York 14627

Received October 13, 2008

Three cyclometalated 6-phenyl-4-(*p*-R-phenyl)-2,2′-bipyridyl (CNN-Ph-R) Pt(II) acetylide complexes, Pt(CNN-Ph-R)(CCPh), where R = Me (**1**), COOMe (**2**), and P(O)(OEt)$_2$ (**3**), have been synthesized and studied. Compounds **1** and **3** have been structurally characterized by single crystal X-ray crystallography and are found to exhibit distorted square planar geometries about the Pt(II) ions. The electrochemical properties of the compounds, as determined by cyclic voltammetry, have also been examined. Complexes **1**−**3** are brightly emissive in fluid CH_2Cl_2 solution and in the solid state with λ_{em}^{max} of ca. 600 nm and lifetimes on the order of ca. 500 ns in fluid solution. The emissions are assigned to a ^{3}MLCT transition. The complexes undergo oxidative quenching by MV^{2+} with quenching rates near the diffusion-controlled limit ($k_q \sim 1.4 \times 10^{10}$ M^{-1} s^{-1}) in CH_2Cl_2 solution. Reductive-quenching experiments of complexes **1**−**3** by the amine donors *N*,*N*,*N*′,*N*′-tetramethylphenylenediamine (TMPD), phenothiazine (PTZ), and *N*,*N*,*N*′,*N*′-tetramethylbenzidine (TMB) follow Stern−Volmer behavior, with very fast quenching rates on the order of 10^9−10^{10} M^{-1} s^{-1} in CH_2Cl_2 solution. When the complexes are employed as the sensitizer in multiple component systems containing MV^{2+}, TEOA, and colloidal Pt in aqueous media, approximately one turnover of H_2 (TN vs mol of chromophore) is produced per hour upon irradiation with $\lambda > 410$ nm but only after at least a 2 h induction period.

Introduction

The conversion of solar energy into chemical energy by artificial photosynthesis remains one of the great challenges in the development of sustainable energy resources for the future.[1−3] The photogeneration of hydrogen from water, which represents the reductive side of water splitting, produces a carbon-free fuel that is storable, clean burning, and most importantly, renewable.[4] Of particular interest is the production of H_2 by molecular photocatalysis.[5] After nearly 30 years since the first reports of multiple component systems containing a metal-complex chromophore (specifically Ru(bpy)$_3^{2+}$, where bpy = 2,2′-bipyridine), an electron relay such as methyl viologen (MV^{2+}), a colloidal platinum catalyst, and a sacrificial electron donor such as ethylenediaminetetraacetic acid (EDTA) were used for the photogeneration of H_2 from water,[6−8] newer but related systems are still emerging. For example, Bernhard et al. recently reported the photoinduced production of H_2 from a multiple component system that contains a heteroleptic iridium(III) sensitizer [Ir(dF(CF$_3$)ppy)$_2$(dtbbpy)]$^+$ (where dF(CF$_3$)ppy = 2-(2,4-difluorophenyl)-5-trifluoromethylpyridine and dtbbpy = 4,4′-di-*tert*-butyl-2,2′-bipyridine), a cobalt(II) complex (Co(bpy)$_3^{2+}$) as the electron-transfer reagent, and triethanolamine (TEOA) as the sacrificial reductant.[9,10] Another account describes the photogeneration ($\lambda = 330$−700 nm) of H_2 from

* To whom correspondence should be addressed. E-mail: eisenberg@chem.rochester.edu.

(1) Lewis, N. S; Nocera, D. G *Proc. Natl. Acad. Sci. U.S.A.* **2006**, *103*, 15729–15735.
(2) Alstrum-Acevedo, J. H.; Brennaman, M. K.; Meyer, T. J. *Inorg. Chem.* **2005**, *44*, 6802–6827.
(3) Eisenberg, R.; Nocera, D. G. *Inorg. Chem.* **2005**, *44*, 6799–6801.
(4) Bard, A. J.; Fox, M. A. *Acc. Chem. Res.* **1995**, *28*, 141–145.
(5) Esswein, A. J.; Nocera, D. G. *Chem. Rev.* **2007**, *107*, 4022–4047.
(6) Keller, P.; Moradpour, A.; Amouyal, E.; Kagan, H. B. *Nouv. J. Chim.* **1980**, *4*, 377–384.
(7) Kiwi, J.; Grätzel, M. *Nature* **1979**, *281*, 657–658.
(8) Lehn, J.-M.; Sauvage, J.-P. *Nouv. J. Chim* **1977**, *1*, 449–451.
(9) Lowry, M. S.; Goldsmith, J. I.; Slinker, J. D.; Rohl, R.; Pascal, R. A., Jr.; Malliaras, G. G.; Bernhard, S. *Chem. Mater.* **2005**, *17*, 5712–5719.
(10) Goldsmith, J. I.; Hudson, W. R.; Lowry, M. S.; Anderson, T. H.; Bernhard, S. *J. Am. Chem. Soc.* **2005**, *127*, 7502–7510.

10.1021/ic801947v CCC: $40.75
Published on Web 04/24/2009

water using zinc−protoporphyrin IX in the presence of colloidal Pt, MV^{2+}, and TEOA.[11] Fukuzumi and co-workers have developed a photocatalytic hydrogen generating system that combines an organic sensitizer, 9-mesityl-10-methylacridinium (Acr^+−Mes), and water soluble Pt nanoclusters functionalized with MV^{2+} in the presence of dihydronicotinamide coenzyme (NADH) as a sacrificial reagent.[12,13] Du et al. showed that Pt(terpyridyl)(acetylide)$^+$ complexes can be employed as the chromophores in multiple component hydrogen-generating systems that contain MV^{2+} or diquat cations DQ^{2+}, where DQ^{2+} is a dialkylated-2,2′-bipyridine, as the electron relay, TEOA, and Pt colloid as the H_2-evolving catalyst.[14,15]

The goal of the current study was to build on the fundamental concepts taken from the seminal work done with $Ru(bpy)_3^{2+}$ and Pt(terpy)(acetylide)$^+$ complexes and examine them in the context of cyclometalated 6-phenyl-2,2′-bipyridyl (CNN) Pt(II) acetylide chromophores. The CNN ligand, similar to 2,2′-6′,2″-terpyridine, and its derivatives have been studied extensively as tridentate chelators in d^6- and d^8-cyclometalated complexes of iridium(III),[16] ruthenium(II),[17,18] palladium(II),[19−21] and platinum(II).[22−27] The Pt(II) CNN complexes are solution luminescent with a desirable ^{3}MLCT excited-state energy.[28,29] The energy of the MLCT absorption band is expected to be lowered relative to Pt(terpy)(acetylide)$^+$ complexes due to the combination of strong acetylide and phenyl carbanion donors that raises the highest occupied molecular orbital (HOMO) localized on the Pt(II) center and a more accepting π^* lowest unoccupied molecular orbital (LUMO) localized on the bipyridyl part of the CNN ligand.

This Article describes the synthesis and characterization of one previously reported and two new cyclometalated Pt(II) CNN acetylide chromophores, **1**−**3**, for the photogeneration of H_2 from water. The CNN ligands **L2** and **L3** with ester groups have been synthesized so that upon hydrolysis the resulting acid will be an effective anchoring group for binding to TiO_2 semiconductor particles,[30] providing an integrated system.[31] In this report, the structural, electrochemical, and photophysical properties of these complexes, as well as oxidative-quenching studies with methyl viologen (MV^{2+}) and reductive-quenching studies with three aryl amine donors, are presented and discussed, as are observations regarding the photogeneration of H_2.

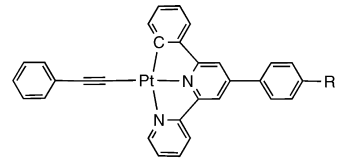

R = CH_3, $COOCH_3$, P(O)$(OEt)_2$

1 **2** **3**

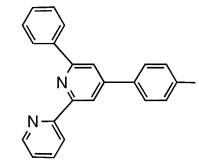

R = $COOCH_3$, P(O)$(OEt)_2$

L2 **L3**

Experimental Section

Characterization and Instrumentation. All NMR spectra were recorded on either Bruker Avance 400 or 500 MHz spectrometers. ^{1}H NMR chemical shifts (in ppm) are referenced using the chemical shift of DMSO-d_6. ^{31}P NMR chemical shifts (in ppm) are relative to an external 85% solution of H_3PO_4 in the appropriate solvent. Mass spectra were measured using a Shimadzu 2010 series liquid chromatograph mass spectrometer (LCMS) operated with an atmospheric pressure chemical ionization (APCI) quadrupole source and the detection of positive and negative ions. The samples were dissolved in CH_2Cl_2 and pumped through the spray chamber using 100% CH_3OH. Elemental analyses were performed by Quantitative Technologies Inc. (QTI). Absorption spectra were recorded using a Hitachi U2000 scanning spectrophotometer (200−1100 nm). Steady-state and frozen emission spectra were obtained using a Spex Fluoromax-P fluorometer corrected for instrument response with monochromators positioned with a 2 nm band-pass. The metal complex concentration of solution samples was 1.0×10^{-5} M in CH_2Cl_2 and each sample was degassed by purging with nitrogen. Solid state emission samples were prepared as a 4% (w/w) mixture of the complex in a matrix of finely ground KBr.

The room temperature emission quantum yields (ϕ_{em}) are measured relative to $Ru(bpy)_3Cl_2$ in degassed H_2O as the reference solution ($\phi_{em} = 0.042$).[32] They were calculated using eq 1

$$\phi_s = \phi_r(I_s/I_r)(A_r/A_s)(n_s^2/n_r^2) \quad (1)$$

where the subscripts s and r, respectively, denote sample and reference; I is the integrated emission intensity; A is the absorbance in a dilute solution ($\sim 10^{-5}$ M, $A < 0.5$) at the wavelength of excitation; and n is the refractive index that corrects for differences between the reference and the sample solutions.[33]

Excited-state lifetime measurements of deoxygenated CH_2Cl_2 solution samples ($\sim 10^{-4}$ M) of complexes **1**−**3** were obtained by

(11) Komatsu, T.; Wang, R.-M.; Zunszain, P. A.; Curry, S.; Tsuchida, E. *J. Am. Chem. Soc.* **2006**, *128*, 16297–16301.
(12) Kotani, H.; Ohkubo, K.; Takai, Y.; Fukuzumi, S. *J. Phys. Chem. B* **2006**, *110*, 24047–24053.
(13) Kotani, H.; Ono, T.; Ohkubo, K.; Fukuzumi, S. *Phys. Chem. Chem. Phys.* **2007**, *9*, 1487–1492.
(14) Du, P.; Schneider, J.; Jarosz, P.; Eisenberg, R. *J. Am. Chem. Soc.* **2006**, *128*, 7726–7727.
(15) Du, P.; Schneider, J.; Jarosz, P.; Zhang, J.; Brennessel, W. W.; Eisenberg, R. *J. Phys. Chem. B* **2007**, *111*, 6887–6894.
(16) Whittle, V. L.; Williams, J. A. G. *Inorg. Chem.* **2008**, *47*, 6596–6607.
(17) Constable, E. C.; Cargill Thompson, A. M. W.; Greulich, S. *J. Chem. Soc., Chem. Commun.* **1993**, 1444–1446.
(18) Collin, J. P.; Beley, M.; Sauvage, J. P.; Barigelletti, F. *Inorg. Chim. Acta* **1991**, *186*, 91–93.
(19) Kim, Y.-J.; Chang, X.; Han, J.-T.; Lim, M. S.; Lee, S. W. *Dalton Trans.* **2004**, 3699–3708.
(20) Lai, S.-W.; Cheung, T.-C.; Chan, M. C. W.; Cheung, K.-K.; Peng, S.-M.; Che, C.-M. *Inorg. Chem.* **2000**, *39*, 255–262.
(21) Mathis, M.; Harsha, W.; Hanks, T. W.; Bailey, R. D.; Schimek, G. L.; Pennington, W. T. *Chem. Mater.* **1998**, *10*, 3568–3575.
(22) Lu, W.; Mi, B.-X.; Chan, M. C. W.; Hui, Z.; Che, C.-M.; Zhu, N.; Lee, S.-T. *J. Am. Chem. Soc.* **2004**, *126*, 4958–4971.
(23) Chan, H.-L.; Ma, D.-L.; Yang, M.; Che, C.-M. *ChemBioChem* **2003**, *4*, 62–68.
(24) Cheung, T.-C.; Cheung, K.-K.; Peng, S.-M.; Che, C.-M. *J. Chem. Soc., Dalton Trans.* **1996**, 1645–1651.
(25) Hofmann, A.; Dahlenburg, L.; van Eldik, R. *Inorg. Chem.* **2003**, *42*, 6528–6538.
(26) Lai, S.-W.; Chan, M. C.-W.; Cheung, T.-C.; Peng, S.-M.; Che, C.-M. *Inorg. Chem.* **1999**, *38*, 4046–4055.
(27) Lai, S. W.; Chan, M. C.-W.; Cheung, K.-K.; Che, C.-M. *Organometallics* **1999**, *18*, 3327–3336.
(28) Lu, W.; Mi, B.-X.; Chan, M. C. W.; Hui, Z.; Zhu, N.; Lee, S.-T.; Che, C.-M. *Chem. Commun.* **2002**, 206–207.
(29) Wu, Z.-X; Wu, L.-Z.; Yang, Q.-Z.; Zhang, L.-P.; Tung, C.-H. *Chin. J. Chem.* **2003**, *21*, 196–199.
(30) Bae, E.; Choi, W.; Park, J.; Shin, H. S.; Kim, S. B.; Lee, J. S. *J. Phys. Chem. B* **2004**, *108*, 14093–14101.
(31) Zhang, J.; Du, P.; Schneider, J.; Jarosz, P.; Eisenberg, R. *J. Am. Chem. Soc.* **2007**, *129*, 7726–7727.
(32) Van Houten, J.; Watts, R. J. *J. Am. Chem. Soc.* **1976**, *98*, 4853–4858.
(33) Morris, J. V.; Mahaney, M. A.; Huber, J. R. *J. Phys. Chem.* **1976**, *80*, 969–974.

frequency doubling and pulse picking a femtosecond Ti-sapphire laser at 450 nm with a 3.8 MHz repetition rate. The laser beam was focused on the samples in a quartz cuvette by a microscope objective (50×, NA 0.55) with a power density of ~1 kW/cm^{-1}. The photoluminescence (PL) from the samples was collected by the same objective and sent through a 0.5 m spectrometer to a charge coupled device (CCD) camera or a time-correlated single photon counting system (~200 ps resolution) for the time-integrated or time-resolved measurements at room temperature. For the time-resolved measurements, the collected PL was spectrally selected by the spectrometer within a narrow bandwidth (~3 nm) so that only the PL decay at the peaks of maximum emission was monitored. The PL decay was measured at 615 nm for complex **1** and 630 nm for complexes **2** and **3**.

Oxidative- and reductive-quenching experiments were done in degassed a CH_2Cl_2 or CH_2Cl_2:CH_3CN (1:4, v/v) solution at room temperature. The process was done by adding small aliquots of standard quencher solution ($MV^{2+}\cdot 2PF_6^-$ in CH_3CN, and TMPD, PTZ, or TMB in CH_2Cl_2) to a solution of **1**, **2**, or **3** at a known concentration (~10^{-5} M). Excess CH_2Cl_2 (~1 mL) was added, and the solution was purged carefully with nitrogen until the original volume was obtained.

Cyclic voltammetry experiments were conducted on an EG&G PAR 263A potentiostat/galvanostat using a three-electrode single compartment cell. A glassy carbon working electrode, a Pt wire auxiliary electrode, and a Ag wire reference electrode were used. For all measurements, samples were dissolved in DMF and degassed with argon. Tetrabutylammonium hexafluorophosphate (Fluka) was used as the supporting electrolyte (0.1 M), and ferrocene (ROC/RIC) was employed as an internal redox reference. All redox potentials are reported relative to the ferrocenium/ferrocene ($Fc^{+/0}$) couple (0.45 V vs SCE[34] and SCE vs NHE = 0.24 V). All scans were done at 100 mV/s unless otherwise noted.

Crystallographic Structure Determinations. Crystals were attached to glass fibers and mounted under a stream of N_2, maintained at 100.0(1) K, on a Bruker SMART platform diffractometer equipped with an APEX II CCD detector, positioned at −33° in 2θ and 5.0 cm from the samples. The X-ray source, powered at 50 kV and 30 mA, provided Mo Kα radiation (λ = 0.71073 Å, graphite monochromator). Preliminary random samplings of reflections were used to determine unit cells and orientation matrices.[35] Complete data collections were obtained by ω scans of 183° (0.5° steps) at four different ϕ settings. Final cell constants were calculated from the xyz centroids of approximately 4000 strong reflections from the actual data collection after integration.[36] The data were additionally scaled and corrected for absorption.[37] Space groups were determined on the basis of systematic absences, intensity statistics, and space group frequencies. Structures were solved by direct or Patterson methods.[38,39] Non-hydrogen atoms were located by difference Fourier syntheses, and their positions were refined with anisotropic displacement parameters, unless noted otherwise, by full-matrix least-squares cycles on F^2.[38] In a similar fashion, all hydrogen atoms were placed geometrically and refined as riding atoms with relative isotropic displacement parameters. The final set of refinement cycles, run to convergence, provided the reported quality assessment parameters.

Details of Photolysis Experiments

Photogeneration of $MV^{+\bullet}$. Each sample was prepared in a 50 mL round-bottom flask with a total volume of 25 mL in CH_2Cl_2. Concentrations of the various components were as follows: 2.7−33.5 mM TEOA, 2.2 × 10^{-5} M chromophore, and 3.1 × 10^{-4} M $MV^{2+}\cdot 2PF_6^-$ unless noted otherwise. About 10 mL of the solution was transferred to a vacuum sealable flask with a quartz cuvette attachment equipped with a stir bar, and the solution was degassed by at least three freeze−pump−thaw cycles. The solution in the cuvette was then irradiated under a 200 W mercury xenon lamp (Oriel) with a 410 nm cutoff filter to remove the high energy light from photolysis, and the absorption spectrum was measured at different time intervals using a Hitachi U2000 scanning spectrophotometer (200−1100 nm).

Photogeneration of H_2. Each sample was prepared in a 50 mL round-bottom flask with a total volume of 25 mL in CH_3CN/H_2O (2:3, v/v). Concentrations of the various components were as follows: 13.4−26.8 mM TEOA, 2.2 × 10^{-5} M chromophore, 6.0 × 10^{-5} M Pt colloid, and 3.1 × 10^{-4} M $MV^{2+}\cdot 2Cl^-$ unless noted otherwise. The pH of the solution was adjusted to pH ~7 using 10% aqueous HCl (v/v). The flask was sealed with a septum and degassed by bubbling N_2 for 20 min under atmospheric pressure at room temperature. After degassing, 5 mL of N_2 was removed with a gastight syringe, and 5 mL of CH_4 (760 Torr) was subsequently added to serve as an internal standard for quantitative GC analysis. The sample was then irradiated under a 200 W mercury xenon lamp (Oriel) with a 410 nm cutoff filter to remove the high energy light from photolysis. The reaction vessel was set up to stir approximately 5 cm in front of the light source in a well-ventilated fume hood. Gas samples (~10 μL) were taken from the headspace of the reaction vessel and injected into the GC using a gastight syringe. The hydrogen generated from the systems was measured by a GC-17A Shimadzu gas chromatograph using nitrogen as the carrier gas with either a molecular sieve 5 Å column (30 m × 0.53 mm) (Supelco) or a molecular sieve column (30 m × 0.530 mm) (J&W Scientific) and a thermal conductivity detector. The amount of H_2 produced was quantified by the ratio of H_2/CH_4 (CH_4 = internal standard), followed by conversion to mL, mol, or turnovers (TNs) of H_2. Turnovers were calculated relative to the amount of chromophore in the system, with errors on the order of ~15% (see Figure S14 in the Supporting Information for example calculations).

Materials. K_2PtCl_4 (VWR), CuI (Aldrich), phenylacetylene (Aldrich), triethylamine (Aldrich), triethanolamine (TEOA) (Aldrich), *N*,*N*,*N*′,*N*′-tetramethylphenylenediamine (TMPD) (Alfa Aesar), phenothiazine (PTZ) (Aldrich), *N*,*N*,*N*′,*N*′-tetramethylbenzidine (TMB) (Aldrich), DMF (Mallinckrodt), and DMSO-d_6 (Cambridge Isotope Laboratories) were purchased commercially and used without further purification. The ligands CNN-Ph-COOMe and CNN-Ph-P(O)(O-

(34) Connelly, N. G.; Geiger, W. E. *Chem. Rev.* **1996**, *96*, 877–910.
(35) *APEX2 V2.1-0*; Bruker AXS: Madison, WI, 2006.
(36) *SAINT V7.34A*; Bruker AXS: Madison, WI, 2006.
(37) Sheldrick, G. M. *SADABS V2004/1*; University of Göttingen: Göttingen, Germany, 2004.
(38) *SHELXTL V6.14*; Bruker AXS: Madison, WI, 2000.
(39) Altomare, A.; Burla, M. C.; Camalli, M.; Cascarano, G. L.; Giacovazzo, C.; Guagliardi, A.; Moliterni, A. G. G.; Polidori, G.; Spagna, R. *SIR97: A New Program for Solving and Refining Crystal Structures*; Istituto di Cristallografia, CNR: Bari, Italy, 1999.

$Et)_2$[40] and complexes [Pt(CNN-Ph-COOMe)Cl], [Pt(CNN-Ph-P(O)$(OEt)_2$)Cl],[40] and [Pt(CNN-Ph-Me)(C≡CPh)] (**1**)[22] were prepared as reported previously. All other solvents and reagents were purchased commercially and used as received unless otherwise noted.

Synthesis and Characterization of New Pt(II) Complexes. [Pt(CNN-Ph-COOMe)(C≡CPh)] (2). To a flask charged with [Pt(CNN-Ph-COOMe)Cl] (101 mg, 0.17 mmol), CuI (11 mg, 5 mg per 50 mg of Pt complex), and phenylacetylene (∼0.06 mL, 0.6 mmol) was added anhydrous DMF (∼15 mL) and NEt_3 (∼5 mL). The mixture was briefly sonicated and then degassed with nitrogen before stirring at room temperature for 2.5 days in the absence of light. The bright orange precipitate was collected by filtration, rinsing with Et_2O until dry. Yield: 108 mg (96%). APCI (*m*/*z*): 662.3, [M + H]. ^{1}H NMR (DMSO-d_6, 400 MHz): δ 9.10 (d, 1H, J = 4.7 Hz), 8.79 (d, 1H, J = 8.0 Hz), 8.67 (s, 1H), 8.43 (m, 2H), 8.28 (d, 2H, J = 8.4 Hz), 8.17 (d, 2H, J = 8.5 Hz), 7.91 (m, 2H), 7.79 (d, 1H, J = 8.2 Hz), 7.39 (d, 2H, J = 7.4 Hz), 7.29 (t, 2H, J = 7.4 Hz), 7.18 (m, 2H), 7.12 (m, 1H), 3.93 (s, 3H, CNN-Ph-CO_2CH_3). FT-IR (neat) ν/cm^{-1}: 2097 ($\nu_{C\equiv C}$), 1713 ($\nu_{C=O}$), 1279 (ν_{C-O}). Anal. Calcd for $C_{32}H_{22}N_2O_2Pt$: C, 58.09; H, 3.35; N, 4.24. Found: C, 54.21; H, 2.53; N, 4.02.

[Pt(CNN-Ph-P(O)$(OEt)_2$)(C≡CPh)] (3). This compound was prepared by the same method as for **2** but on a smaller scale using [Pt(CNN-Ph-P(O)$(OEt)_2$)Cl] (50 mg, 0.073 mmol), CuI (5 mg), phenylacetylene (∼0.03 mL, 0.27 mmol), DMF (∼6 mL), and NEt_3 (∼2 mL), stirring under nitrogen for four days at room temperature. Addition of Et_2O to the reaction solution caused precipitation of an orange product. At times, the precipitate formed was green due to Pt−Pt stacking interactions.[41,42] The precipitate was collected by filtration, rinsing with Et_2O until dry. Yield: 50 mg (94%). APCI (*m*/*z*): 740.2, [M + H]. ^{1}H NMR (DMSO-d_6, 500 MHz): δ 9.11 (d, 1H), 8.77 (d, 1H, J = 8.0 Hz), 8.64 (s, 1H), 8.42 (m, 2H), 8.26 (d, 2H, J = 4.4 Hz), 7.91 (m, 4H), 7.80 (d, 1H, J = 7.6 Hz), 7.39 (d, 2H, J = 7.3 Hz), 7.29 (t, 2H, J = 7.5 Hz), 7.18 (m, 2H), 7.12 (t, 1H, J = 6.8 Hz), 4.09 (m, 4H, CNN-Ph-P(O)$(OCH_2CH_3)_2$), 1.28 (t, 6H, 7.0 Hz, CNN-Ph-P(O)$(OCH_2CH_3)_2$). ^{31}P{^{1}H} NMR (DMSO-d_6, 202 MHz): δ 17.08 (s). FT-IR (neat) ν/cm^{-1}: 2097 ($\nu_{C\equiv C}$), 1248 ($\nu_{P=O}$). Anal. Calcd for $C_{34}H_{29}N_2O_3PPt$: C, 55.21; H, 3.95; N, 3.79. Found: C, 53.01; H, 4.03; N, 4.46.

Results and Discussion

Synthesis and Characterization. Complexes **1**−**3** were prepared by the reaction of their [Pt(CNN)Cl] precursors with phenylacetylene in the presence of triethylamine and catalytic CuI following a previously reported procedure.[43] The complexes have been characterized by ^{1}H and ^{31}P NMR spectroscopies, mass spectrometry (APCI), FT-IR, and elemental analyses, as well as by single crystal X-ray crystallography for complexes **1** and **3**. The elemental analyses for complexes **2** and **3** are not satisfactory; the low percent carbon is due in part to difficulties getting complete combustion of the complexes under experimental conditions.

Crystal Structure Determination. Crystals of **1** suitable for single crystal X-ray diffraction were grown by slow evaporation of a dichloromethane solution of the complex, while crystals for complex **3** were obtained by slow diffusion of diethyl ether into a dichloromethane solution of the compound. ORTEP diagrams of complexes **1** and **3** are shown in Figures 1 and 2, respectively. The unit cell, data collection, and refinement parameters are summarized in Table 1 with selected bond lengths and angles for both structures given in Table 2. Both complexes exhibit distorted square planar coordination geometries around the Pt(II) nucleus. For complexes **1** and **3,** the Pt−N distances to the central pyridine and the Pt−C(acetylide) distances, 1.980(5) and 1.990(3) Å and 1.980(6) and 1.976(3) Å, respectively, are slightly shorter than the peripheral Pt−N and Pt−C(aryl) distances of 2.090(6) and 2.122(3) Å and 2.028(6) and 1.992(3) Å, respectively. These values are consistent with earlier reports of analogous structures having the general formula Pt(pbpy)(C≡CR) (pbpy = 6-phenyl-2,2′-bipyridine, R = C_6H_5, 4-MeC_6H_4, C_6F_5, $SiMe_3$, C≡CC_6H_5, C≡C$SiMe_3$, C≡C−C≡C$SiMe_3$, 9,9-Me_2-fluorene, and 9-Me-carbazole).[22,28,44] In those reported structures, the Pt−C(acetylide) distances range between 1.956 and 1.98 Å, the Pt−N bond to the central pyridine is shorter than the Pt−N bond to the peripheral pyridine ring, and the Pt−C(aryl) bonds are in the expected range of ∼2.0 Å.

In the crystal structure of complex **1**, there exists infinite stacks of complexes that have weak alternating Pt···π and π···π interactions with interplanar distances in the range of 3.3−3.4 Å. The Pt···π interaction involves Pt from one molecule and the π system of a bipyridine ligand unit from a neighboring molecule (Figure 1). In a similar fashion, the π···π stacking involves the phenyl ring of the ligand core from one molecule and the central pyridine ring of the CNN ligand in a nearest-neighbor molecule. In the crystal structure of complex **3**, there is one cocrystallized ether solvent molecule per Pt complex. Pyridyl rings of symmetry equivalent molecules are involved in π···π stacking with distances of 3.4−3.5 Å, but no intermolecular Pt···Pt contacts are observed (Figure 2); the nearest Pt···Pt distance is 4.95 Å.

Electrochemistry. The cyclic voltammograms of complexes **1**−**3** (see Supporting Information) were measured in 0.1 M n-BuNPF_6 in DMF, and the electrochemical data were summarized in Table 3. All of the redox potentials are reported relative to NHE with the ferrocenium/ferrocene ($Fc^{+/0}$) couple used as an internal redox standard and a value of 0.45 V vs SCE taken for the $Fc^{+/0}$ couple[34] and a value of 0.24 V taken for SCE vs NHE. Each complex exhibits two reductions, assigned to the CNN ligand. The first CNN-based reduction observed at −1.08,

(40) Schneider, J.; Du, P.; Wang, X.; Brennessel, W. W.; Eisenberg, R. *Inorg. Chem.* **2009**, *48*, 1498–1506.
(41) Bailey, J. A.; Hill, M. G.; Marsh, R. E.; Miskowski, V. M.; Schaefer, W. P.; Gray, H. B. *Inorg. Chem.* **1995**, *34*, 4591–4599.
(42) Herber, R. H.; Croft, M.; Coyer, M. J.; Bilash, B.; Sahiner, A. *Inorg. Chem.* **1994**, *33*, 2422–2426.
(43) Chakraborty, S.; Wadas, T. J.; Hester, H.; Flaschenreim, C.; Schmehl, R.; Eisenberg, R. *Inorg. Chem.* **2005**, *44*, 6284–6293.
(44) Seneclauze, J. B.; Retailleau, P.; Ziessel, R. *New J. Chem.* **2007**, *31*, 1412–1416.

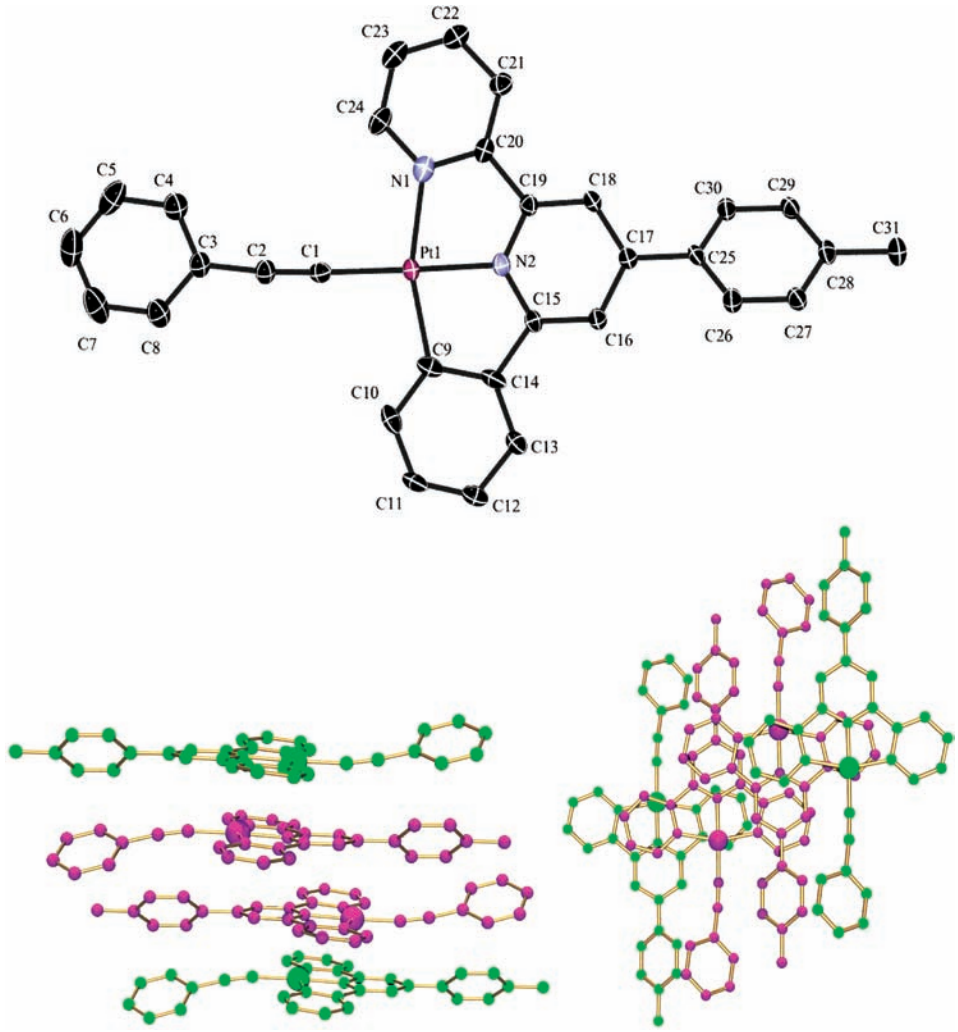

Figure 1. (Top) ORTEP drawing of complex **1**, hydrogen atoms omitted for clarity. (Bottom) Two views of the intermolecular stacking of complex **1**, showing the infinite alternating Pt$\cdots\pi$ (green and pink molecules) and $\pi\cdots\pi$ stacking interactions (pink molecules).

−1.01, and −1.00 V (vs NHE), for **1**, **2**, and **3**, respectively, is reversible, while the second ligand-based reduction observed at −1.67, −1.48, and −1.50 V, respectively, is quasi-reversible. Complex **1** with R = Me is the most difficult to reduce while **2** and **3** are slightly easier to reduce and have similar reduction potentials, consistent with the electron donating/withdrawing ability of the pendant R group (Me in **1**, COOMe and $P(O)(OEt)_2$ in **2** and **3**, respectively). In an earlier report by Che et al., the reduction potentials for several Pt(pbpy)(acetylide) complexes were measured in CH_2Cl_2 solution and only one reduction was observed, possibly due to a different solvent window than for the current study, attributed to a one-electron reduction of the CNN ligand.[22] In that report, the authors observe similar electronic effects with a complex having an electron-withdrawing COOEt pendant group possessing a reduction potential of −1.60 V (vs $Fc^{+/0}$), while a complex containing two *tert*-butyl groups underwent a more difficult reduction at −1.93 V.

The oxidation waves of complexes **1**−**3** correspond to two irreversible oxidations. The first oxidation observed at +0.94 V (vs NHE) is the same for complexes **1**−**3** and has tentatively been assigned to a $Pt^{II/III}$ process.[43] The second oxidation at +1.48, +1.52, and +1.23 V for complexes **1**−**3**, respectively, follows no obvious trend and is therefore uncertain in assignment. In an earlier report by Che and coworkers, the authors only observed one irreversible oxidation for the Pt(pbpy)(acetylide) complexes in CH_2Cl_2, which was not assigned.[22]

Absorption and Emission Spectra. The photophysical data for complexes **1**−**3** are summarized in Tables 4 and 5. Complexes **2** and **3** show steady-state electronic spectra similar to that of complex **1** in CH_2Cl_2 solution (Figure 3), which has been discussed elsewhere.[22,29] The UV region of the absorption spectra are dominated by intraligand (IL) transitions with maxima at ca. 285, 340, and 370 nm, having molar absorpivities (ε) on the order of 10 000 $dm^3\ mol^{-1}\ cm^{-1}$. In the visible region of the absorption spectra of complexes **1**−**3**, there is a broad charge-transfer maximum at ca. 440 nm with a slight shoulder at ca. 460 nm that has been previously assigned to a metal-to-ligand charge-transfer (^{1}MLCT) transition.[22,28]

All of the Pt(CNN)(CCPh) complexes are brightly luminescent in dichloromethane solution at room temperature and at 77 K, in frozen MeOH:EtOH (1:4, v/v) glass, and in the solid state. The steady-state emission maxima in fluid CH_2Cl_2

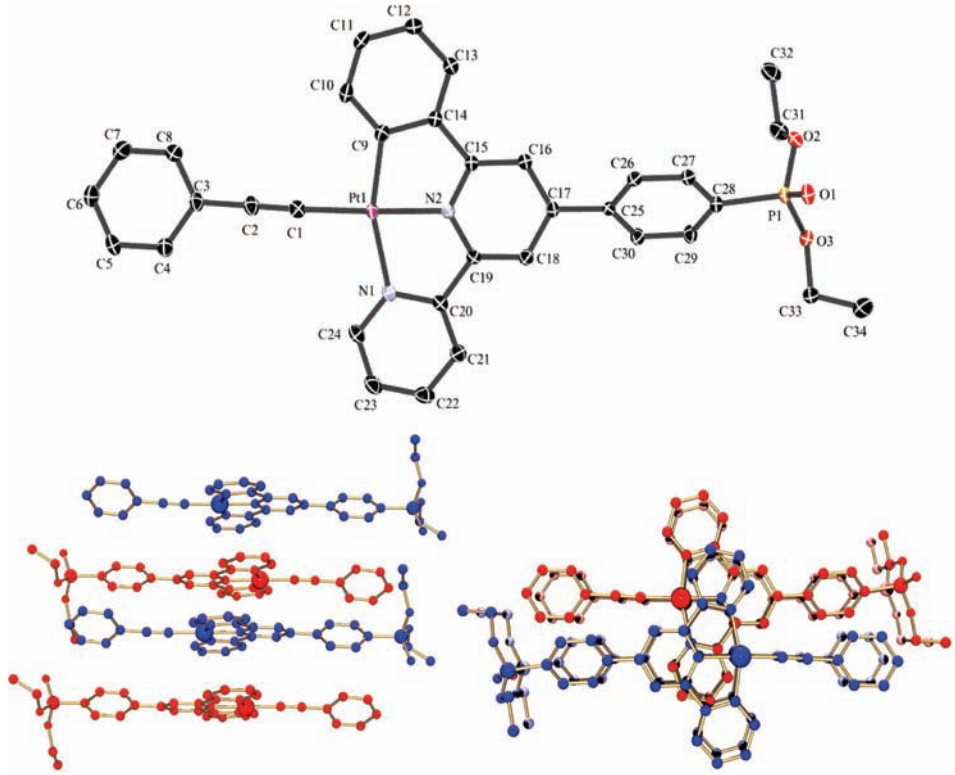

Figure 2. (Top) ORTEP drawing of complex **3**, hydrogen atoms omitted for clarity. (Bottom) Two views of the intermolecular stacking of complex **3**, showing the pyridyl rings of symmetry equivalent molecules involved in $\pi\cdots\pi$ stacking interactions.

Table 1. Unit Cell, Data Collection, and Refinement Parameters for Complex **1** and Complex **3**·Et_2O

	complex **1**	complex **3**·Et_2O
formula	$C_{31}H_{22}N_2Pt$	$C_{34}H_{29}N_2O_3PPt\cdot Et_2O$
fw	617.60	813.77
T (K)	100.0(1)	100.0(1)
λ (Å)	0.71073	0.71073
crystal system	monoclinic	monoclinic
space group	$P2_1/c$	$C2/c$
a (Å)	9.579(2)	32.340(4)
b (Å)	23.142(5)	6.9509(9)
c (Å)	11.254(3)	31.480(4)
α (deg)	90	90
β (deg)	114.928(3)	110.027(2)
γ (deg)	90	90
V (Å^3)	2262.3(9)	6648.4(14)
Z	4	8
ρ_{cald} (mg/m^3)	1.813	1.626
μ (mm^{-1})	6.225	4.313
crystal color	orange needle	orange needle
crystal size (mm^3)	0.22 × 0.08 × 0.04	0.38 × 0.14 × 0.04
θ range (deg)	2.18−32.57	1.38−32.03
no. of data	8163	11527
no. of parameters	296	419
GOF[a]	1.178	1.207
$R1$, $wR2$ (F^2, $I > 2\sigma(I)$)[b]	0.0534, 0.1024	0.0377, 0.0725
$R1$, $wR2$ (F^2, all data)[b]	0.0691, 0.1071	0.0539, 0.0814

[a] GOF $= S = [\sum w(F_o^2 - F_c^2)^2/(m - n)]^{1/2}$, where m = number of reflections and n = number of parameters. [b] $R1 = \sum||F_o| - |F_c||/\sum|F_o|$. $wR2 = [\sum w(F_o^2 - F_c^2)^2/\sum w(F_o^2)^2]^{1/2}$, where $w = 1/[\sigma^2(F_o)^2 + (aP) + bP]$ and $P = 1/3\ \max(0, F_o^2) + (2/3)F_c^2$.

Table 2. Selected Bond Lengths (Å) and Angles (deg) for Complexes **1** and **3**·Et_2O

	Complex **1**		
Pt(1)−N(1)	2.090(6)	Pt(1)−C(1)	1.980(6)
Pt(1)−N(2)	1.980(5)	Pt(1)−C(9)	2.028(6)
C(1)−C(2)	1.197(8)		
N(2)−Pt(1)−N(1)	79.3(2)	N(2)−Pt(1)−C(9)	81.0(2)
C(9)−Pt(1)−C(9)	160.3(2)	C(1)−Pt(1)−N(2)	177.5(2)
C(1)−C(2)−C(3)	172.8(7)		
C(16)−C(17)−C(25)−C(26)	37.1(8)		
	Complex **3**·Et_2O		
Pt(1)−N(1)	2.122(3)	Pt(1)−C(1)	1.976(3)
Pt(1)−N(2)	1.990(3)	Pt(1)−C(9)	1.992(3)
C(1)−C(2)	1.201(5)		
N(2)−Pt(1)−N(1)	78.38(11)	N(2)−Pt(1)−C(9)	81.87(12)
C(1)−Pt(1)−N(2)	178.22(12)	C(9)−Pt(1)−N(1)	160.19(12)
C(1)−C(2)−C(3)	177.4(4)		
C(16)−C(17)−C(25)−C(26)	38.1(4)		

Table 3. Electrochemical Data for Complexes **1**−**3** and Quenching Reagents, As Determined by Cyclic Voltammetry[a]

complex/reagent	$E_{1/2}^{red}$/V	$E_{1/2}^{ox}$/V
1	−1.08, −1.67[b]	+0.94,[c] +1.48[c]
2	−1.01, −1.48[b]	+0.94,[c] +1.52[c]
3	−1.00, −1.50[b]	+0.94,[c] +1.23[c]
$MV^{2+}\cdot 2PF_6^-$	−0.20, −0.58	
TMPD		+0.39
PTZ		+0.83
TMB		+0.84
TEOA		+1.12,[c] +1.43[c]

[a] All redox potentials are reported versus NHE relative to the ($Fc^{+/0}$) couple (0.45 V vs SCE[34] and SCE vs NHE = 0.24 V). [b] Quasi-reversible under experimental conditions. [c] Irreversible under experimental conditions.

solution for complexes **1**−**3** are 595, 607, and 606 nm, with excited-state lifetimes determined to be 485, 550, and 605 ns, respectively (λ_{ex} = 450 nm), and quantum yields (ϕ_{em}) between 0.047 and 0.073 measured relative to $Ru(bpy)_3Cl_2$ in H_2O (ϕ_{em} = 0.042).[32] The emissive state in **1**−**3** has been assigned to a ^{3}MLCT transition.[20,29,45] Complexes **2** and **3** have slightly red-shifted emission maxima compared with complex **1**, due to the electron-withdrawing ester groups on

(45) Lai, S.-W.; Che, C.-M. *Top. Curr. Chem.* **2004**, *241*, 27–63 (Transition Metal and Rare Earth Compounds III).

Table 4. Spectroscopic and Photophysical Data for Phenylacetylide Complexes

complex	λ_{abs}/nm (ε/dm^3 mol^{-1} cm^{-1})	solution λ_{em}/nm[a,b]	τ/ns[b]	ϕ_{em}[c]
1	283 (42 520), 337 (19 980), 370 (14 570), 441 (9950), 460 (9670)	595 (max), 645 (sh)	485	0.073
2	289 (44 940), 340 (16 730), 373 (12 510), 448 (8450), 461 (8380)	607 (max), 645 (sh)	550	0.049
3	287 (43 040), 340 (13 780), 373 (9820), 447 (6380), 464 (6300)	606 (max), 645 (sh)	605	0.047

[a] 1.0×10^{-5} M in CH_2Cl_2. [b] $\lambda_{ex} = 440$ nm. [c] Emission quantum yields measured relative to $Ru(bpy)_3Cl_2$ in H_2O ($\phi_{em} = 0.042$).[32]

Table 5. Solid State and Frozen Emission Data, $\lambda_{ex} = 440$ nm

complex	frozen solution λ_{em}/nm[a]	frozen glass λ_{em}/nm[b]	solid state λ_{em}/nm[c]
1	560 (max), 595, 625, 690	545, 580 (max), 625	590 (max), 625 (sh)
2	575 (max), 605, 650	560, 605 (max), 660	610 (max), 650 (sh)
3	570 (max), 605, 650	555 (max), 585, 640	600 (max), 640 (sh)

[a] CH_2Cl_2, 77 K. [b] MeOH:EtOH (1:4, v/v), 77 K. [c] 4% (w/w) mixture with KBr, rt.

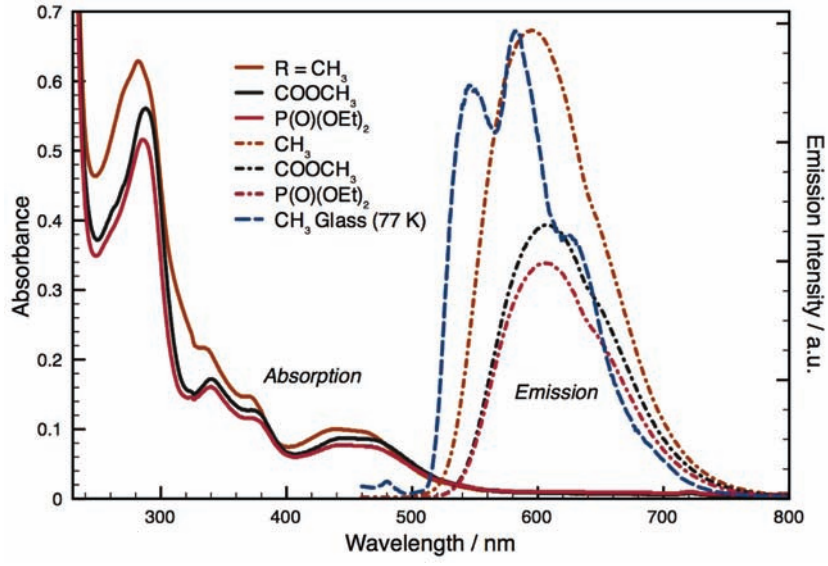

Figure 3. Steady-state absorption and emission spectra of complexes **1**−**3** in fluid CH_2Cl_2 solution (1.0×10^{-5} M), and normalized frozen glass (MeOH/EtOH, 1:4 v/v) emission spectrum of complex **1** (blue dashed).

the CNN ligand. Similar to the electrochemical results, this observation is consistent with the idea that the LUMO, which is localized on the CNN ligand, is slightly lower in energy for complexes **2** and **3** compared with the LUMO energy for complex **1**.

In frozen CH_2Cl_2 solution, the emission spectra for complexes **1**−**3** are broad, exhibiting little structure in the range of 550−750 nm, with maxima at ca. 570 nm. However, the frozen MeOH:EtOH (1:4, v/v) glass emission spectra of complexes **1**−**3** have structured emission profiles that span the range of ca. 525−725 nm (Figure 3 and Figure S2 in the Supporting Information). From the frozen glass emission, an estimation of the excited-state energy of the MLCT emissive state, E_{00}, can be made.[46] The E_{00} energies for complexes **1**−**3** were estimated directly from the highest energy emission maxima in the frozen glass samples and were calculated to be 2.28, 2.22, and 2.23 eV, respectively. This method is an alternative to the more thorough derivation of E_{00} using a single-mode, Franck−Condon analysis of emission spectral profiles.[47−50]

The emission maxima of complexes **1**−**3** in the solid state at room temperature exhibit similar behavior to the steady-state emission spectra in fluid solution, with complexes **2** and **3** having slightly red-shifted emission maxima compared with complex **1**. Their solid state emission maxima of 590, 610, and 600 nm, are accompanied by shoulders at 625, 650, and 640 nm, for **1**, **2**, and **3**, respectively.

Excited-State Potentials. The excited-state reduction and oxidation potentials may be estimated using eqs 2 and 3, respectively, where E^* is the excited-state reduction ($E_{1/2}{}^{*red}$) or oxidation ($E_{1/2}{}^{*ox}$) potential, E is the ground-state reduction ($E_{1/2}{}^{red}$) or oxidation ($E_{1/2}{}^{ox}$) potential as determined electrochemically, and w_r is an electrostatic work term describing charge generation and separation within the electron-transfer complex.[51]

$$E_{1/2}{}^{*red} = E_{1/2}{}^{red} + E_{00} + w_r \quad (2)$$

$$E_{1/2}{}^{*ox} = E_{1/2}{}^{ox} - E_{00} + w_r \quad (3)$$

For simple estimations of the excited-state potentials of the complexes in this study, the work terms for these neutral

(46) Turro, N. J. *Modern Molecular Photochemistry*; Addison-Wesley Publishing Co.: Reading, MA, 1978; 628 pp.
(47) Caspar, J. V.; Meyer, T. J. *J. Am. Chem. Soc.* **1983**, *105*, 5583–5590.
(48) Claude, J. P.; Meyer, T. J. *J. Phys. Chem.* **1995**, *99*, 51–54.
(49) Dattelbaum, D. M.; Omberg, K. M.; Schoonover, J. R.; Martin, R. L.; Meyer, T. J. *Inorg. Chem.* **2002**, *41*, 6071–6079.
(50) Kober, E. M.; Caspar, J. V.; Lumpkin, R. S.; Meyer, T. J. *J. Phys. Chem.* **1986**, *90*, 3722–3734.
(51) Jones, J. W. E.; Fox, M. A. *J. Phys. Chem.* **1994**, *98*, 5095–5099.

Table 6. Estimated Excited-State Energies and Excited-State Redox Potentials

complex	E_{00}/eV	$E_{1/2}{}^{*red}$/V	E^{*ox}/V
1	2.28	+1.20	−1.34
2	2.22	+1.21	−1.28
3	2.23	+1.23	−1.29

Table 7. Oxidative and Reductive Quenching of Complexes **1**−**3** by MV^{2+} and by TMPD, PTZ, and TMB, Respectively

complex	$k_q(MV^{2+})/10^{10}$ M^{-1} s^{-1}	k_q(TMPD)/10^{10} M^{-1} s^{-1}	k_q(PTZ)/10^9 M^{-1} s^{-1}	k_q(TMB)/10^9 M^{-1} s^{-1}
1	1.4	1.7	8.1	10.6
2	1.9	1.5	7.2	8.2
3	1.1	1.4	7.9	6.9

complexes can be assumed to be zero. For the excited-state oxidation potential E^{*ox}, only a rough estimate can be obtained since the one electron oxidation process is irreversible from an electrochemical standpoint. While only a rough estimate, the E^{*ox} value thus calculated is useful for comparing the series of complexes **1**−**3** in the current study.

$$E_{1/2}{}^{*red} = E_{1/2}{}^{red} + E_{00} \quad (4)$$

$$E^{*ox} = E^{ox} - E_{00} \quad (5)$$

From eqs 4 and 5, complexes **1**−**3** have estimated $E_{1/2}{}^{*red}$ values of +1.20, +1.21, and +1.23 V (vs NHE, Table 6), respectively, and E^{*ox} values estimated at −1.34, −1.28, −1.29 V, respectively. When these excited-state potentials are compared to those reported for analogous Pt(terpyridyl)(acetylide)$^+$ compounds ($E_{1/2}{}^{*red}$ ca. +1.8 V vs NHE and E^{*ox} ca. −1.1 V),[15,52] complexes **1**−**3** are substantially weaker excited-state oxidants and slightly stronger excited-state reductants.

Oxidative-Quenching Studies. Complexes **1**−**3** were all found to undergo oxidative quenching by MV^{2+} in CH_2Cl_2 solution, following Stern−Volmer behavior.[53] The rates of quenching are essentially diffusion controlled with k_q values of 1.4, 1.9, and 1.1 × 10^{10} M^{-1} s^{-1} for complexes **1**−**3**, respectively (Table 7). These results are comparable to an earlier report of the analogous Pt(ttpy)(CCPh)$^+$ complex that exhibits oxidative quenching by MV^{2+} and a number of diquat cations DQn^{2+}, where DQn^{2+} is a dialkylated-2,2′-bipyridine for n = 1 (ethylene bridge), 2 (propylene), and 3 (butylene), with k_q values of 3.3 × 10^9 M^{-1} s^{-1} for oxidative quenching by MV^{2+} and 10.0, 7.1, and 6.1 × 10^9 M^{-1} s^{-1} for oxidative quenching by $DQ1^{2+}$, $DQ2^{2+}$, and $DQ3^{2+}$ respectively, in CH_3CN/H_2O solution.[15]

The neutral complexes **1**−**3** have faster oxidative-quenching rates than does the cationic Pt(ttpy)(CCPh)$^+$ complex, ∼1.0 × 10^{10} vs ∼1.0 × 10^9 M^{-1} s^{-1}, respectively. Complexes **1**−**3** are slightly stronger excited-state reductants than Pt(ttpy)(CCPh)$^+$, with excited-state oxidation potentials of ∼−1.3 V (vs NHE, Table 6), compared with an excited-state oxidation potential of −1.14 V for Pt(ttpy)(CCPh)$^+$.[15] With the assumption that the ground-state reduction potential

Table 8. Electrochemical Driving Force for the Quenching Reaction Estimated Using the Excited-State Oxidation and Reduction Potentials of Complexes **1**−**3**

	$\Delta E°$ for quenching reagent/V				
complex	MV^{2+}	TEOA[a]	TMPD	PTZ	TMB
1	1.14	0.08	0.81	0.37	0.36
2	1.08	0.09	0.82	0.38	0.37
3	1.09	0.11	0.84	0.40	0.39

[a] Emission quenching of complexes not observed.

of MV^{2+} is −0.20 V (vs NHE, Table 3), the driving force, $\Delta E°$, for complexes **1**−**3** to undergo oxidative quenching by MV^{2+} is ∼1.1 V (vs NHE, Table 8), while $\Delta E°$ for Pt(ttpy)(CCPh)$^+$ to undergo oxidative quenching by MV^{2+} is 0.94 V. The difference in $\Delta E°$ for the two systems is only 0.16 V, but it can explain the approximate 10-fold difference in quenching rate constants k_q based on the simple Marcus theory. The Marcus expression for the free energy of activation, $\Delta G^‡$, of an outer sphere electron transfer is given in eq 6. The ratio of the rates of two reactions from the Eyring theory, assuming both have the same prefactor, is given by eq 7, and the difference in the free energies of activation, $\Delta\Delta G^‡$, assuming the same reorganization energy λ for the two reactions, is found in eq 8.

$$\Delta G^‡ = \frac{(\lambda + \Delta G^o)^2}{4\lambda} \quad (6)$$

$$\frac{k_1}{k_2} = e^{-(\Delta G_2{}^‡ - \Delta G_1{}^‡)/RT} \quad (7)$$

$$\Delta G_2{}^‡ - \Delta G_1{}^‡ = \Delta\Delta G^‡ = \frac{\{2\lambda(\Delta G_2{}^o - \Delta G_1{}^o) + ((\Delta G_2{}^o)^2 - (\Delta G_1{}^o)^2)\}}{4\lambda} \quad (8)$$

While values of λ for electron-transfer reactions involving complexes such as **1**−**3** and Pt(ttpy)(CCPh)$^+$ have not been determined, we use as an estimate 0.5 eV that was suggested for electron-transfer-quenching reactions of the Pt(II) complex Pt(Ph_2phen)(ecda) (where Ph_2phen = 4,7-diphenylphenanthroline and ecda = 1-(ethoxycarbonyl)-1-cyanoethylene-2,2-dithiolate).[54] On the basis of this value of λ and a difference in driving force for the two quenching reactions of 0.16 V, values for the ratio of rates ranged up to a value of 13 depending on how far the driving force difference was from the actual value of λ. We do not know the relative positions of these electron-transfer reactions in the nomal Marcus region but think that the difference in the quenching rate can be rationalized primarily on this basis. Additionally, it is also possible that the change in k_q is due in part to the difference in charge between the cationic Pt(ttpy)(CCPh)$^+$ and the neutral complexes **1**−**3**, with slower k_q values for the dynamic quenching of cationic Pt(ttpy)(CCPh)$^+$ by the dicationic MV^{2+} compared with faster quenching of the neutral complexes by MV^{2+}.

Reductive-Quenching Studies. Contrary to earlier reports of analogous Pt(terpyridyl)(acetylide)$^+$ complexes that un-

(52) Narayana-Prabhu, R.; Schmehl, R. H. *Inorg. Chem.* **2006**, *45*, 4319–4321.
(53) Vincze, L.; Sándor, F.; Pém, J.; Bosnyák, G. *J. Photochem. Photobiol., A* **1999**, *120*, 11–14.
(54) Bevilacqua, J. M.; Eisenberg, R. *Inorg. Chem.* **1994**, *33*, 1886–1890.

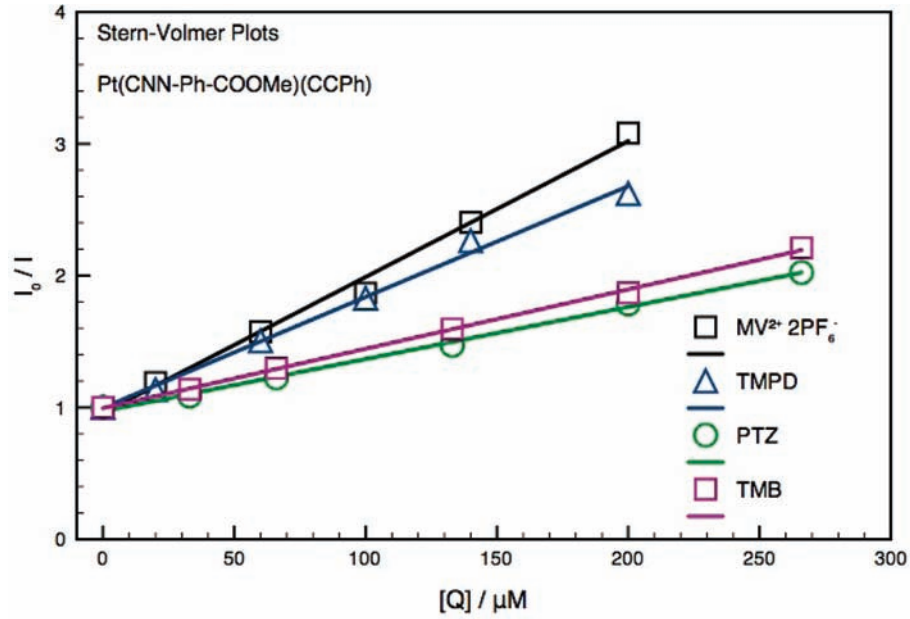

Figure 4. Stern−Volmer plots of oxidative and reductive quenching of complex **2** by MV^{2+}, TMPD, PTZ, and TMB in a CH_2Cl_2 solution.

dergo reductive quenching by triethanolamine (TEOA) with quenching rates on the order of 1.7×10^9 M^{-1} s^{-1} in CH_3CN/H_2O solution,[14,15] none of the Pt CNN complexes in this study show emission quenching by TEOA in CH_2Cl_2 solution. Complexes **1**−**3** are weaker excited-state oxidants than their terpyridyl analogues, with estimated $E_{1/2}{}^{*red}$ values of ∼+1.2 V (vs NHE, Table 6) for complexes **1**−**3**, compared with estimated $E_{1/2}{}^{*red}$ values of ∼+1.8 V for the Pt(terpyridyl)(acetylide)$^+$ complexes.[15,52] Whereas the $\Delta E°$ for complexes **1**−**3** to undergo reductive quenching by TEOA (E^{ox} = +1.12 V vs NHE, Table 3) is estimated at only ∼0.1 V (Table 8), $\Delta E°$ for the Pt(terpyridyl)(acetylide)$^+$ complexes is estimated to be significantly higher at ∼0.7 V. For comparison, Pt(ttpy)(CCPh)$^+$ undergoes reductive quenching with TEOA with a k_q value of 1.4×10^9 M^{-1} s^{-1} in CH_3CN/H_2O solution.[14,15]

In contrast to the absence of quenching with TEOA, complexes **1**−**3** do undergo emission quenching with the aryl amines *N*,*N*,*N*′,*N*′-tetramethylphenylenediamine (TMPD), phenothiazine (PTZ), and *N*,*N*,*N*′,*N*′-tetramethylbenzidine (TMB), which oxidize more easily than TEOA and are known to reductively quench the emission of derivatives of $Ru(bpy)_3{}^{2+}$ (bpy = 2, 2′-bipyridine)[55] and Pt(terpyridyl)(acetylide)$^+$ complexes.[52] For complexes **1**−**3**, reductive quenching by TMPD, PTZ, and TMB in CH_2Cl_2 solution follows Stern−Volmer behavior with k_q values at or near the diffusion-controlled limit (Figure 4, Table 7). That complexes **1**−**3** are quenched by TMPD, PTZ, and TMB, but not TEOA, can be conjectured in terms of $\Delta E°$, values of which are summarized in Table 8. For quenching by TMPD, $\Delta E°$ is ∼0.8 V with k_q values of $\sim 1.4 \times 10^{10}$ M^{-1} s^{-1} for complexes **1**−**3**. The emission quenching of complexes **1**−**3** by PTZ and TMB, have a $\Delta E°$ that is less at ∼0.4 V, with slightly slower k_q values of $\sim 8 \times 10^9$ M^{-1} s^{-1}. These data suggest that a $\Delta E°$ of ∼0.1 V, which is that of quenching by TEOA, does not have sufficient driving force to generate reductive-emission quenching with **1**−**3**.

Photoreduction of MV^{2+} and H_2 Production. Though there was no reductive quenching of complexes **1**−**3** by TEOA, it was found that in a deoxygenated system containing one of the Pt(CNN) complexes (**1**, **2**, or **3**), MV^{2+}, and TEOA in CH_2Cl_2 solution, the blue $MV^{+\bullet}$ radical anion develops within 5 min of irradiation with $\lambda > 410$ nm light (Figure 5). This is comparable to similar systems containing Pt(terpyridyl)(acetylide)$^+$ chromophores, MV^{2+}, and TEOA in CH_3CN/H_2O solution, which are capable of generating $MV^{+\bullet}$ within 5 min as well. In the current report, it was found that $MV^{+\bullet}$ generation in the system was dependent on TEOA concentration, with an optimum [TEOA] of 27 mM, as determined by monitoring the increasing [$MV^{+\bullet}$] at 604 nm with time-resolved UV/vis spectroscopy (Figure S6 in the Supporting Information). On the basis of the fact that reductive quenching of complexes **1**−**3** by TEOA does not occur, the concentration of $MV^{+\bullet}$ in the system will approach a limiting value with respect to the Pt complex chromophore if the latter, once oxidized photochemically by MV^{2+}, is not reduced by TEOA.

It has been reported by Du et al. that visible-light photolysis ($\lambda > 410$ nm) of Pt(terpyridyl)(acetylide)$^+$ chromophores in CH_3CN/H_2O in the presence of MV^{2+}, TEOA, and colloidal Pt leads to the photogeneration of H_2.[14,15] Analogous experiments with complexes **1**−**3** used in place of Pt(terpyridyl)(acetylide)$^+$ chromophores also lead to the photogeneration of H_2 but at much slower rates and in much lower quantities (Figure 6). While the reported system with Pt(terpyridyl)(acetylide)$^+$ chromophores are capable of generating H_2 in less than 30 min, at least two hours of irradiation are required of the analogous systems with complexes **1**, **2**, or **3** as sensitizers under the same experimental conditions. Furthermore, the systems with complexes

(55) Calvert, J. M.; Caspar, J. V.; Binstead, R. A.; Westmoreland, T. D; Meyer, T. J. *J. Am. Chem. Soc.* **1982**, *104*, 6620–6627.

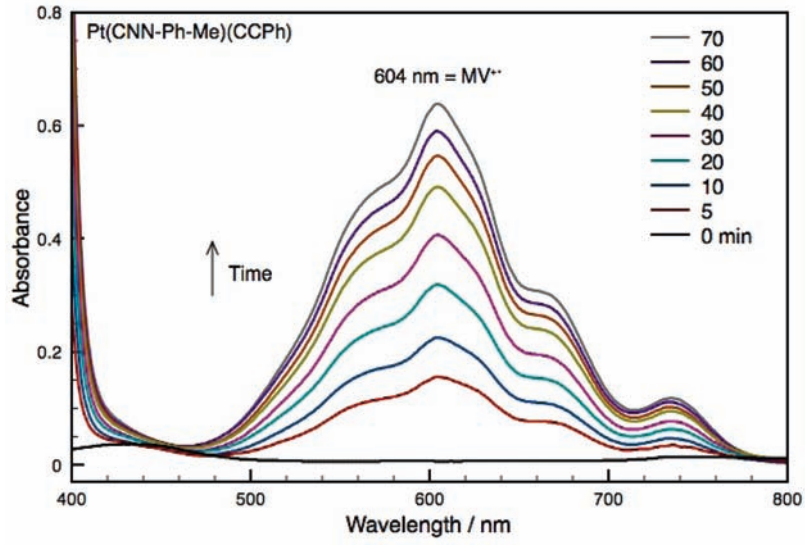

Figure 5. UV−vis monitoring of the generation of $MV^{+\bullet}$ in a system that contains 2.2×10^{-5} M complex **1**, 3.1×10^{-4} M MV^{2+}, and 26.8 mM TEOA in a CH_2Cl_2 solution, irradiating with $\lambda > 410$ nm light.

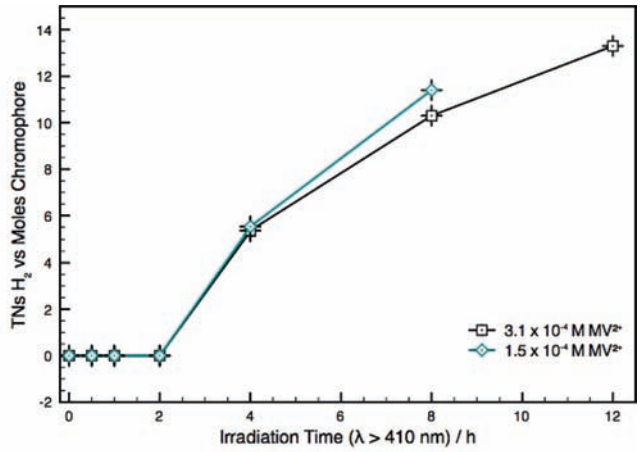

Figure 6. Hydrogen production using 2.2×10^{-5} M complex **3**, $(1.5-3.1) \times 10^{-4}$ M MV^{2+}, and 26.8 mM TEOA in a CH_3CN/H_2O solution, irradiating with $\lambda > 410$ nm light. Notice the induction period.

1−**3** as chromophores yield only ∼12 turnovers (TNs per mol of chromophore) of H_2 after 12 h of photolysis, an average of ∼1 TN/h of irradiation, which is much poorer than results obtained with Pt(terpyridyl)(acetylide)$^+$ chromophores of more than 800 TNs of H_2 after 20 h of photolysis with $\lambda > 410$ nm.[15] Moreover, systems containing a CNN chromophore, **1**, **2**, or **3**, in CH_3CN/H_2O solution required substantially longer irradiation times (∼35 min) to generate the intense blue coloration of $MV^{+\bullet}$ obtained in analogous Pt(terpyridyl)(acetylide)$^+$-based systems after only 5 min of irradiation. While the low TNs of H_2 in systems that contain **1** or **2** as sensitizers may be a possible consequence of their low solubilities in CH_3CN/H_2O resulting in heterogeneous systems, complex **3** has good solubility in CH_3CN/H_2O, and therefore its meager H_2 photogeneration cannot be rationalized in the same way.

Instead, a different explanation can be drawn on the basis of consideration of a reaction scheme for hydrogen-generating systems containing Pt CNN chromophores (C) in eqs 9−15. Key differences of this scheme from that put forward previously for the Pt terpyridyl acetylide chromophore are the absence of (1) reductive quenching by TEOA and (2) subsequent electron transfer from reduced chromophore C^- to MV^{2+}. It is also possible that unproductive back-electron transfer between C^+ and $MV^{+\bullet}$ occurs more readily than with the Pt terpyridyl acetylide systems and that reduction of C^+, produced upon oxidative quenching, proceeds more slowly by TEOA than the corresponding reaction in the Pt terpyridyl acetylide systems, since in those latter systems, the oxidized chromophore is dicationic and more strongly oxidizing.

$$C \xrightarrow{h\nu} C^* \quad (9)$$

$$C^* + MV^{2+} \longrightarrow C^+ + MV^{+\cdot} \quad (10)$$

$$C^+ + MV^{+\cdot} \longrightarrow C + MV^{2+} \quad (11)$$

$$C^+ + TEOA \longrightarrow C + TEOA^+ \quad (12)$$

$$TEOA^+ \xrightarrow{-H^+} TEOA\cdot \xrightarrow[MV^{+\cdot}]{MV^{2+}} CH_2(OH)CHO + NH(EtOH)_2 \quad (13)$$

$$n\,MV^{+\cdot} + Pt_{coll} \longrightarrow Pt_{coll}^{n-} + n\,MV^{2+} \quad (14)$$

$$2\,H_2O \xrightarrow{Pt_{coll}^{n-}} H_2 + 2\,OH^- \quad (15)$$

The consequence of these differences is a lower flux of electrons from $MV^{+\bullet}$ to the colloidal Pt catalyst which functions essentially as a microelectrode for H_2 generation.[4,56,57] The induction period thus represents the time needed to make the electrode potential on the Pt catalyst sufficiently negative for proton reduction to occur, and the slow rate of H_2 formation indicates that the electron flow into the Pt catalyst via eq 14 is substantially lower than that obtained in the Pt terpyridyl acetylide systems reported earlier. While TEOA is capable of transferring a second and highly reducing electron during its decomposition (eq 15),[14] it needs to lose one electron before this can happen. It thus appears that for productive hydrogen-generating systems on

(56) Miller, D.; McLendon, G. *Inorg. Chem.* **1981**, *20*, 950–953.
(57) Kiwi, J.; Grätzel, M. *J. Am. Chem. Soc.* **1979**, *101*, 7214–7217.

the basis of the Pt CNN chromophores, a more strongly reducing sacrificial donor, one more easily oxidized than TEOA, is needed.

Conclusions

The structural, electrochemical, and photophysical properties of two new cyclometalated Pt(II) CNN acetylide complexes have been examined in detail and compared with a closely related but previously reported complex. Two of the complexes were characterized by single crystal X-ray crystallography, exhibiting a distorted square planar coordination geometry around the Pt(II) nucleus. The complexes are brightly emissive in fluid CH_2Cl_2 solution and in the solid state at ~600 nm, and their emissions are assigned to a ^{3}MLCT charge-transfer excited-state. In CH_2Cl_2 solution the compounds undergo fast oxidative quenching by MV^{2+} and fast reductive quenching by three aryl amine donors, with quenching rates near the diffusion-controlled limit for both. However, the complexes do not undergo reductive quenching by TEOA. When complexes **1**−**3** are employed as photosensitizers in a multiple component system containing MV^{2+}, colloidal Pt, and TEOA, a 2 h induction period for H_2 formation is seen and only modest amounts of H_2 are evolved (~1 TN/h). The sluggish performance in the photogeneration of H_2 relates to a low flux of electrons into the Pt colloidal catalyst, which in turn results from the absence of reductive quenching and slow regeneration of the chromophore after oxidative quenching.

Acknowledgment. This work was supported by the Department of Energy, Division of Basic Sciences (DE-FG02-90ER14125). The authors also wish to acknowledge the following support from the University of Rochester: Graduate Assistance in Areas of National Need (GAANN) Fellowships (J.S. and P.J.), Elon Huntington Hooker Fellowship (P.D.), and Weissberger Memorial Fellowship (J.S.). The authors also thank Prof. Todd Krauss for help in making possible the excited-state lifetime measurements.

Supporting Information Available: Emission spectra, Stern−Volmer plots, generation of $MV^{+\bullet}$ as dependent on TEOA concentration, emission spectra of quenching experiments, cyclic voltammograms, and example calculations of TNs H_2 vs mol of chromophore. This material is available free of charge via the Internet at http://pubs.acs.org.

IC801947V